

Analysis of effective temperature and kinetic freeze-out volume in high energy nucleus-nucleus and proton-proton collisions

Muhammad Waqas^{1,*}, Fu-Hu Liu^{1,†}, Li-Li Li^{1,‡}, Haidar Mas'ud Alfanda^{2,§}

¹*Institute of Theoretical Physics & State Key Laboratory of Quantum Optics and Quantum Optics Devices, Shanxi University, Taiyuan 030006, China*

²*Key Laboratory of Quark & Lepton Physics (MOE) and Institute of Particle Physics, Central China Normal University, Wuhan 430079, China*

Abstract: The transverse momentum spectra of different types of particles produced in central and peripheral gold-gold (Au-Au) and (inelastic) proton-proton (pp) collisions at the Relativistic Heavy Ion Collider (RHIC), as well as in central and peripheral lead-lead (Pb-Pb) and pp collisions at the Large Hadron Collider (LHC) are analyzed by the standard distribution in terms of multi-component. The obtained results from the standard distribution give an approximate agreement with the measured experimental data by the STAR, PHENIX and ALICE Collaborations. The methodical behavior of the effective temperature and kinetic freeze-out volume with the mass dependence for different particles is obtained, which observes the early kinetic freeze-out of heavier particles as compared to the lighter particles. Furthermore, the kinetic freeze-out volumes for different particles are observed to be different, which reveals a direct signature of the mass dependent differential kinetic freeze-out. It is also observed that the peripheral nucleus-nucleus (AA) and pp collisions at the same center-of-mass energy per nucleon pair are almost equivalent in terms of the extracted effective temperature.

Keywords: Transverse momentum spectra, effective temperature, kinetic freeze-out volume

PACS: 12.40.Ee, 14.40.Aq, 24.10.Pa, 25.75.Ag

1 Introduction

A hot and dense fireball is assumed to form for a brief period of time (\sim a few fm/ c) over an extended region after the initial collision, which undergoes a collective expansion and both the temperature and volume or density of the system change. Three types of temperatures namely the initial temperature, chemical freeze-out temperature and kinetic freeze-out temperature can be found in the literature, which describe the excitation degrees of interacting system at the stages of initial collision, chemical freeze-out and kinetic freeze-out respectively [1, 2, 3, 4, 5]. There is another type of temperature, named the effective temperature, which is not a real temperature and it describes the sum of excitation degree of the interacting system and the effect of transverse flow at the stage of kinetic freeze-out.

Usually, the initial stage of collision happens earlier,

followed by the chemical and kinetic freeze-out stages successively. Similarly, the initial temperature is the largest and the kinetic freeze-out temperature is the lowest among the three real temperatures, while the chemical freeze-out temperature is in between the initial and kinetic freeze-out temperatures. It does not get rid of the simultaneity for chemical and kinetic freeze-outs, which results in the chemical and kinetic freeze-out temperatures to be the same. The effective temperature is often larger than the kinetic freeze-out temperature but it is equal to kinetic freeze-out temperature in case of zero transverse flow velocity.

To conceive the given nature of the nuclear force and to break the system into massive fragments [6, 7], it is a good way to bring the nucleons in interactions in nucleus-nucleus (AA) collisions at intermediate and high energies and such a process provokes a liquid-gas

*E-mail: waqas_phy313@yahoo.com

†Corresponding author. E-mail: fuhuliu@163.com; fuhuliu@sxu.edu.cn

‡E-mail: shanxi-lll@qq.com

§E-mail: hmasud@mails.ccnuc.edu.cn

type phase transition. In AA collisions at higher energies, a phase transition from hadronic matter to quark-gluon plasma (QGP) is expected to occur. The volume occupied by such ejectiles source where the mutual nuclear interactions become negligible (they only feel the coulombic repulsive force and are free from the attractive force) is said to be kinetic freeze-out volume and it has been introduced in various statistical and thermodynamic models [8, 9]. The kinetic freeze-out volume gives information of the co-existence of phase transition. This is one of the major quantities, which is important in the extraction of vital observables such as multiplicity, micro canonical heat capacity and its negative branch or shape of caloric curves under the external constraints [10, 11, 12, 13, 14].

It is conceivable that the volume of interacting system increases from the initial state to the latest kinetic freeze-out stage. The study of dependences of effective temperature and kinetic freeze-out volume on collision energy, event centrality, system size and particle rapidity is very attractive and is a huge project. We are very interested in the effective temperature and kinetic freeze-out volume in central and peripheral AA and (inelastic) proton-proton (pp) collisions at the Relativistic Heavy Ion Collider (RHIC) and the Large Hadron Collider (LHC) over a wide enough energy range in which QGP is expected to form.

In this paper, we study the dependence of effective temperatures in central and peripheral gold-gold (Au-Au) and lead-lead (Pb-Pb) collisions at the RHIC and LHC energies and compare their peripheral collisions with pp collisions of the same center-of-mass energy per nucleon pair $\sqrt{s_{NN}}$ (or the center-of-mass energy \sqrt{s} for pp collisions). Only 62.4 GeV at the RHIC and 5.02 TeV at the LHC are considered. By way of parenthesis, the kinetic freeze-out volumes are obtained. We present the approach of effective temperature and kinetic freeze-out volume from the transverse momentum spectra of the identified particles produced in the mentioned AA and pp collisions.

The remainder of this paper is structured as follows. The formalism and method are described in Section 2. Results and discussion are given in Section 3. In Section 4, we summarize our main observations and conclusions.

2 The method and formalism

Generally, two main processes of particle production are under consideration, which includes the soft exci-

tation and hard excitation processes. The soft excitation process has numerous choices of formalisms, including but are not limited to the Hagedorn thermal model (Statistical-bootstrap model) [15], the (multi-)standard distribution [16], the Tsallis and related distributions with various formalisms [17], the blast wave model with Tsallis statistics [18], the blast wave model with Boltzmann statistics [19, 20, 21, 22], and other thermodynamic related models [23, 24, 25, 26]. The hard excitation process has very limited choice of formalisms and can be described by the theory of strong interaction [27, 28, 29].

The experimental data of the transverse momentum spectrum of the particles are fitted by using the standard distribution which is the combination of Boltzmann, Fermi-Dirac and Bose-Einstein with spin $S = 0, +1$ and -1 respectively. The standard distribution at the mid-rapidity can be demonstrated as [16]

$$f_S(p_T) = \frac{1}{N} \frac{dN}{dp_T} = \frac{1}{N} \frac{gV}{(2\pi)^2} p_T \sqrt{p_T^2 + m_0^2} \times \left[\exp\left(\frac{\sqrt{p_T^2 + m_0^2}}{T}\right) + S \right]^{-1} \quad (1)$$

in which the chemical potential is neglected, where N is the experimental number of considered particles, T is the fitted effective temperature, V is the fitted kinetic freeze-out volume (in terms of interaction volume) of the emission source at the stage of kinetic freeze-out, $g = 3$ (or 2) is the degeneracy factor for pion and kaon (or proton), and m_0 is the rest mass of the considered particle. As a probability density function, the integral of Eq. (1) is naturally normalized to 1, i.e., we have $\int_0^{p_{T\max}} f_S(p_T) dp_T = 1$, where $p_{T\max}$ denotes the maximum p_T .

Considering the experimental rapidity range $[y_{\min}, y_{\max}]$ around the mid-rapidity, we have the accurate form of Eq. (1) to be

$$f_S(p_T) = \frac{1}{N} \frac{gV}{(2\pi)^2} p_T \int_{y_{\min}}^{y_{\max}} \left(\sqrt{p_T^2 + m_0^2} \cosh y - \mu \right) \times \left[\exp\left(\frac{\sqrt{p_T^2 + m_0^2} \cosh y - \mu}{T}\right) + S \right]^{-1} dy, \quad (2)$$

where the chemical potential μ is particle dependent, which was studied by us recently [30]. In high energy collisions, μ_j ($j = \pi, K$, and p) are less than several MeV, which affects slightly V comparing with that for $\mu_j = 0$. Then, we may regard $\mu \approx 0$ in Eq. (2) at high energies considered in the present work. In Eqs. (1) and (2), only T and V are free parameters.

Usually, we have to use the two-component standard distribution because single component standard distribution is not enough for the simultaneous description of very low- and low- p_T regions, which are contributed by the resonance decays and other soft excitation processes respectively. More than two or multi-component standard distribution can also be used in some cases. We have the simplified multi-component (l -component) standard distribution to be

$$f_S(p_T) = \sum_{i=1}^l k_i \frac{1}{N_i} \frac{gV_i}{(2\pi)^2} p_T \sqrt{p_T^2 + m_0^2} \times \left[\exp\left(\frac{\sqrt{p_T^2 + m_0^2}}{T_i}\right) + S \right]^{-1}, \quad (3)$$

where N_i and k_i denote respectively the particle number and fraction contributed by the i -th component, and T_i and V_i denote respectively the effective temperature and kinetic freeze-out volume corresponding to the i -th component.

More accurate form of l -component standard distribution can be written as,

$$f_S(p_T) = \sum_{i=1}^l k_i \frac{1}{N_i} \frac{gV_i}{(2\pi)^2} p_T \times \int_{y_{\min}}^{y_{\max}} \left(\sqrt{p_T^2 + m_0^2} \cosh y - \mu \right) \times \left[\exp\left(\frac{\sqrt{p_T^2 + m_0^2} \cosh y - \mu}{T_i}\right) + S \right]^{-1} dy. \quad (4)$$

In Eqs. (3) and (4), only T_i , V_i and k_i ($i \leq l-1$) are free parameters. Generally, $l = 2$ or 3 is enough for describing the spectra in a not too wide p_T range.

In fact, Eqs. (1) or (2) and (3) or (4) can be used for the description of p_T spectra and for the extraction of effective temperature and kinetic freeze-out volume in very low- and low- p_T regions. The high- p_T region contributed by the hard excitation process has to be fitted by the Hagedorn function [15] which is an inverse power law

$$f_H(p_T) = \frac{1}{N} \frac{dN}{dp_T} = A p_T \left(1 + \frac{p_T}{p_0} \right)^{-n} \quad (5)$$

which is resulted from the perturbative QCD (quantum chromodynamics) [27, 28, 29], where A is the normalization constant, which depends on free parameters p_0 and n , and it results in $\int_0^{p_T^{\max}} f_H(p_T) dp_T = 1$.

In case of considering the contributions of both the soft and hard excitation processes, we use the superpo-

sition in principle

$$f_0(p_T) = k f_S(p_T) + (1-k) f_H(p_T), \quad (6)$$

where k is the contribution ratio of the soft process and gives a natural result in $\int_0^{p_T^{\max}} f_0(p_T) dp_T = 1$. In Eq. (6), the contribution of soft process is from 0 to $\sim 2-3$ GeV/ c and the hard component contributes the whole p_T range. There are some mixtures between the contributions of the two processes.

According to the Hagedorn model [15], the contributions of the two processes can be separated completely. One has another superposition

$$f_0(p_T) = A_1 \theta(p_1 - p_T) f_S(p_T) + A_2 \theta(p_T - p_1) f_H(p_T), \quad (7)$$

where $\theta(x)$ is the usual step function, and A_1 and A_2 are the normalization constants which make $A_1 f_S(p_1) = A_2 f_H(p_1)$. Equation (7) gives the contribution of soft process from 0 to p_1 , while the hard component contributes from p_1 up to the maximum.

We will use only the first component in Eq. (7) due to the reason, we do not study a very wide p_T range in the present work. In the case of neglecting the contribution of hard component in low- p_T region in Eq. (6), the first component in Eq. (6) gives the same result as the first component in Eq. (7). In fact, Eq. (4) with $l = 2$, that is the two-component standard distribution, is used in the present work.

3 Results and discussion

Figure 1 demonstrates the transverse momentum spectra, $(1/2\pi p_T) d^2 N / dp_T dy$, of the negatively charged particles π^- , K^- and \bar{p} produced in (a) central (0-10%) and (b) peripheral (40-80%) Au-Au collisions at $\sqrt{s_{NN}} = 62.4$ GeV. The circles, triangles and squares represent the experimental data measured in the mid-rapidity range $-0.5 < y < 0$ at the RHIC by the STAR Collaboration [31]. The curves are our fitted results by Eq. (4) with $l = 2$. Following each panel, the results of Data/Fit are presented. The values of the related parameters along with the χ^2/ndof (χ^2 and number of degree of freedom) are given in Table 1. It can be seen that the two-component standard distribution fits approximately the experimental data measured at mid-rapidity in Au-Au collisions at the RHIC.

The transverse momentum spectra $(1/N_{ev}) d^2 N / dp_T dy$ of π^- , K^- and \bar{p} produced in (a) central (0-5%) and (b) peripheral (80-90%) Pb-Pb collisions at $\sqrt{s_{NN}} = 5.02$

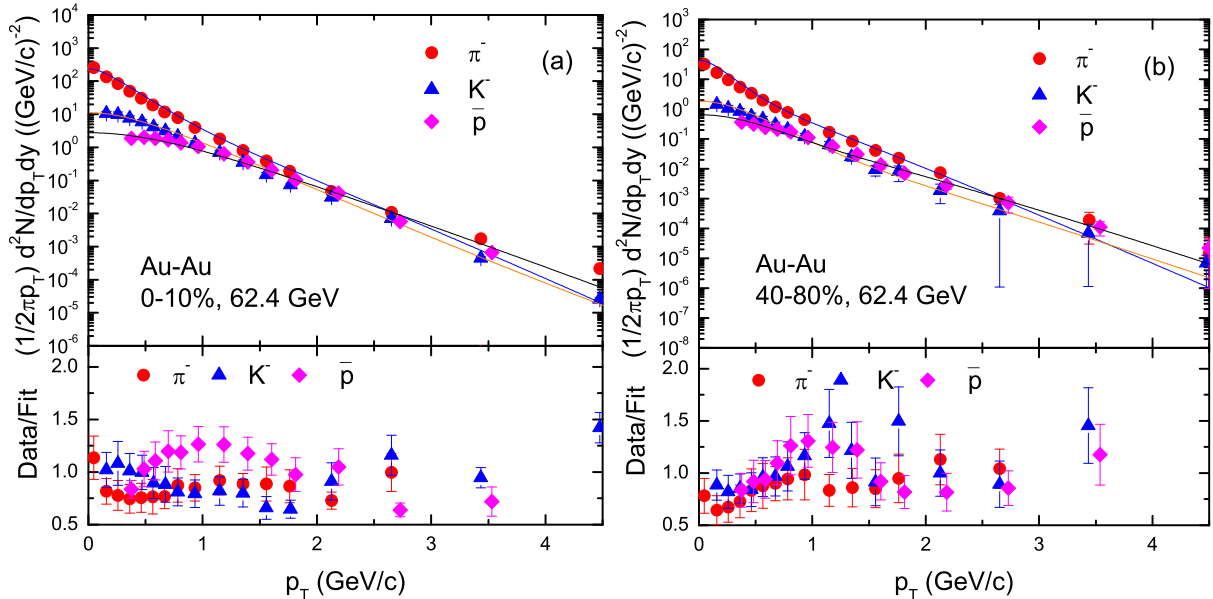


Fig. 1. Transverse momentum spectra of π^- , K^- and \bar{p} produced in (a) central (0–10%) and (b) peripheral (40–80%) Au-Au collisions at $\sqrt{s_{NN}} = 62.4$ GeV. The symbols represent the experimental data measured in the mid-rapidity range $-0.5 < y < 0$ at the RHIC by the STAR Collaboration [31]. The curves are our fitted results by Eq. (4) with $l = 2$. Following each panel, the results of Data/Fit are presented.

TeV are shown in Fig. 2, where N_{ev} on the vertical axes of panels (a) and (b) denote the number of events. The experimental data of π^- , K^- and \bar{p} measured in mid-rapidity range $|y| < 0.5$ at the LHC by the ALICE Collaboration [32] are represented by the circles, triangles and squares respectively. The curves are our results fitted by Eq. (4) with $l = 2$. Following each panel, the results of Data/Fit are presented. The values of the related parameters along with the χ^2/ndof are given in Table 1. One can see that the two-component standard distribution fits approximately the experimental data measured at mid-rapidity in Pb-Pb collisions at the LHC.

Figures 3(a) and 3(b) show the transverse momentum spectra, $E d^3\sigma/dp^3 = (1/2\pi p_T) d^2\sigma/dp_T dy$, of π^- , K^- and \bar{p} produced in pp collisions at $\sqrt{s} = 62.4$ GeV and 5.02 TeV respectively, where E and σ on the vertical axes of panels (a) and (b) denote the energy and cross-section respectively. The symbols represent the experimental data measured in the mid-rapidity range $|\eta| < 0.35$ by the PHENIX Collaboration [33] and in the mid-rapidity range $|y| < 0.5$ by the ALICE Collaborations [32]. The curves are our results fitted by Eq. (4) with $l = 2$. Following each panel, the results of Data/Fit are presented. The values of the related parameters along with the χ^2/ndof are given in Table 1. One can see that the two-component distribu-

tion fits approximately the experimental data measured at mid-rapidity in pp collisions at the RHIC and LHC.

To study the change trends of parameters with the rest mass of the particles, Figure 4 shows the dependences of effective temperature T on rest mass m_0 for productions of negative charged particles in central and peripheral (a) Au-Au collisions at 62.4 GeV and (b) Pb-Pb collisions at 5.02 TeV, while pp collisions at (a) 62.4 GeV and (b) 5.02 TeV are also studied and compared to peripheral AA collisions of the same energy (per nucleon pair). The filled, empty and half filled symbols represent central and peripheral AA and pp collisions respectively. One can see that the effective temperature T is larger in central AA collisions as compared to peripheral AA collisions, and peripheral AA collisions are comparable with the pp collisions at the same $\sqrt{s_{NN}}$ (\sqrt{s}). The mass differential scenario is observed, as the effective temperature T increases with the increase of rest mass of particles. The present work conforms various mass differential scenarios [2, 3, 18, 34, 35].

Figure 5(a) shows the dependences of kinetic freeze-out volume V on rest mass m_0 for productions of negative charged particles in central and peripheral Au-Au collisions at $\sqrt{s_{NN}} = 62.4$ GeV as well as in pp collisions at $\sqrt{s} = 62.4$ GeV, while Fig. 5(b) gives the dependences of V on m_0 for negative charged particles produced in central and peripheral Pb-Pb colli-

Table 1. Values of free parameters (T_1 , T_2 , V_1 , V_2 and k), normalization constant (N_0 for Figs. 1 and 2 or σ_0 for Fig. 3) and χ^2/ndof corresponding to the solid curves in Figs. 1–3.

| Collisions | Centrality | Particle | T_1 (GeV) | T_2 (GeV) | V_1 (fm ³) | V_2 (fm ³) | k | N_0 (σ_0 (mb)) | χ^2/ndof |
|-------------------------------|------------|-------------------|-------------------|-------------------|--------------------------|--------------------------|-------------------|--------------------------|----------------------|
| Fig. 1 Au-Au 62.4 GeV | 0–10% | π^- | 0.141 ± 0.008 | 0.268 ± 0.007 | 2036 ± 193 | 2395 ± 210 | 0.72 ± 0.07 | 0.10 ± 0.01 | 68/16 |
| | | K^- | 0.239 ± 0.009 | 0.317 ± 0.007 | 1314 ± 110 | 1411 ± 120 | 0.70 ± 0.05 | 0.033 ± 0.005 | 49/16 |
| | | \bar{p} | 0.280 ± 0.012 | 0.314 ± 0.004 | 796 ± 70 | 911 ± 84 | 0.60 ± 0.10 | 0.025 ± 0.005 | 43/16 |
| | 40–80% | π^- | 0.100 ± 0.006 | 0.250 ± 0.006 | 906 ± 97 | 1325 ± 170 | 0.70 ± 0.06 | 0.025 ± 0.004 | 57/16 |
| | | K^- | 0.179 ± 0.008 | 0.317 ± 0.004 | 634 ± 50 | 581 ± 40 | 0.70 ± 0.05 | 0.0070 ± 0.0010 | 10/16 |
| | | \bar{p} | 0.201 ± 0.007 | 0.302 ± 0.005 | 304 ± 40 | 341 ± 15 | 0.59 ± 0.09 | 0.0010 ± 0.0020 | 6/16 |
| Fig. 2 Pb-Pb 5.02 TeV | 0–5% | π^- | 0.257 ± 0.017 | 0.574 ± 0.005 | 3699 ± 500 | 2081 ± 180 | 0.93 ± 0.08 | 2.37 ± 0.10 | 395/36 |
| | | K^- | 0.344 ± 0.014 | 0.410 ± 0.006 | 1801 ± 235 | 2111 ± 110 | 0.93 ± 0.03 | 0.72 ± 0.33 | 820/36 |
| | | \bar{p} | 0.459 ± 0.014 | 0.512 ± 0.006 | 1101 ± 165 | 1011 ± 88 | 0.95 ± 0.09 | 0.33 ± 0.01 | 748/36 |
| | 80–90% | π^- | 0.120 ± 0.009 | 0.374 ± 0.004 | 1791 ± 145 | 1229 ± 66 | 0.70 ± 0.09 | 0.078 ± 0.004 | 549/36 |
| | | K^- | 0.198 ± 0.016 | 0.560 ± 0.005 | 775 ± 95 | 1321 ± 70 | 0.90 ± 0.05 | 0.020 ± 0.001 | 124/36 |
| | | \bar{p} | 0.202 ± 0.018 | 0.480 ± 0.006 | 1201 ± 120 | 401 ± 41 | 0.42 ± 0.07 | 0.0080 ± 0.0010 | 148/36 |
| Fig. 3(a) pp 62.4 GeV | π^- | 0.112 ± 0.006 | 0.220 ± 0.004 | 38 ± 4 | 80 ± 6 | 0.84 ± 0.04 | 1.40 ± 0.10 | 42/22 | |
| | K^- | 0.160 ± 0.007 | 0.310 ± 0.006 | 32 ± 4 | 17 ± 2 | 0.73 ± 0.03 | 0.194 ± 0.020 | 10/16 | |
| | \bar{p} | 0.235 ± 0.008 | 0.230 ± 0.006 | 9 ± 2 | 11 ± 2 | 0.77 ± 0.20 | 0.156 ± 0.016 | 89/26 | |
| Fig. 3(b) pp 5.02 TeV | π^- | 0.188 ± 0.008 | 0.487 ± 0.005 | 42 ± 4 | 137 ± 6 | 0.80 ± 0.05 | 0.32 ± 0.11 | 992/36 | |
| | K^- | 0.200 ± 0.013 | 0.490 ± 0.004 | 8 ± 3 | 180 ± 6 | 0.80 ± 0.07 | 0.081 ± 0.018 | 866/36 | |
| | \bar{p} | 0.239 ± 0.010 | 0.511 ± 0.005 | 22 ± 4 | 56 ± 4 | 0.60 ± 0.06 | 0.045 ± 0.004 | 583/36 | |

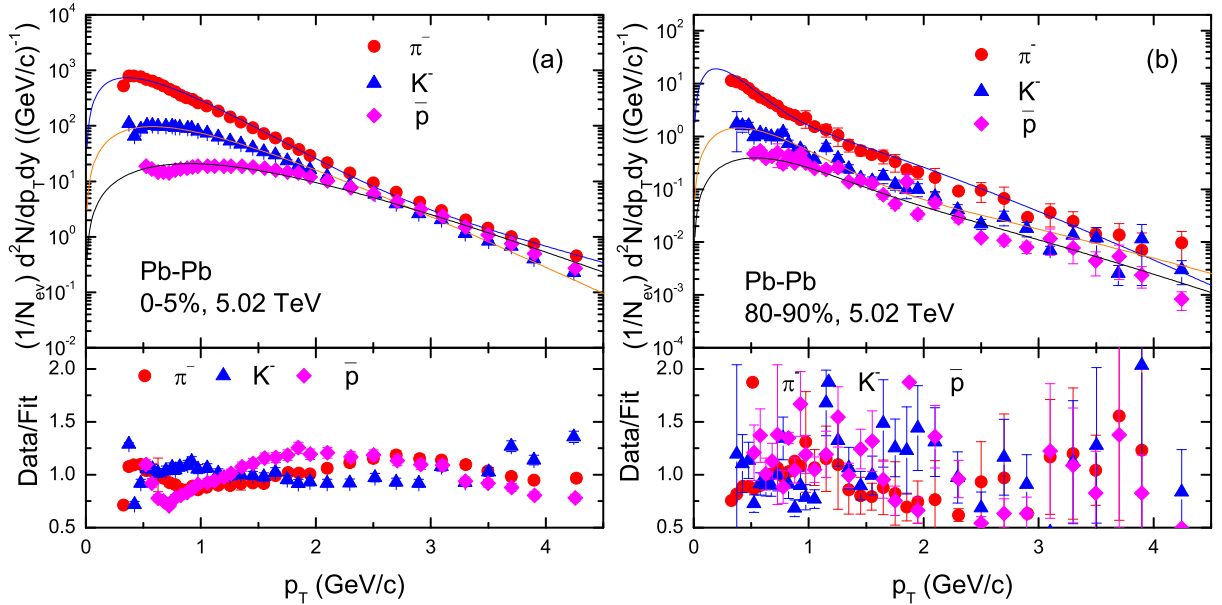


Fig. 2. Transverse momentum spectra of π^- , K^- and \bar{p} produced in (a) central (0–5%) and (b) peripheral (80–90%) Pb-Pb collisions at $\sqrt{s_{NN}} = 5.02$ TeV. The symbols represent the experimental data measured in the mid-rapidity range $|y| < 0.5$ at the LHC by the ALICE Collaboration [32]. The curves are our results fitted by Eq. (4) with $l = 2$. Following each panel, the results of Data/Fit are presented.

sions at $\sqrt{s_{NN}} = 5.02$ TeV as well as in pp collisions at $\sqrt{s} = 5.02$ TeV. The filled, empty and half filled symbols represent the central AA, peripheral AA and pp collisions respectively and they represent the results weighted different contribution fractions in two components listed in Table 1. It can be seen that the kinetic freeze-out volumes in central AA collisions for all the particles in Figs. 5(a) and 5(b) are larger than those in peripheral AA collisions, which shows large numbers of

participants in central AA collisions as compared to peripheral AA collisions. This also indicates to a system of quicker approach of equilibrium in central AA collisions than in peripheral AA collisions. The kinetic freeze-out volume in pp collisions is much less than that in peripheral AA collisions of the same $\sqrt{s_{NN}}$ (\sqrt{s}), which is caused by the much less participant nucleons in pp collisions. It is also observed that the kinetic freeze-out volume decreases with the increase of the rest mass of

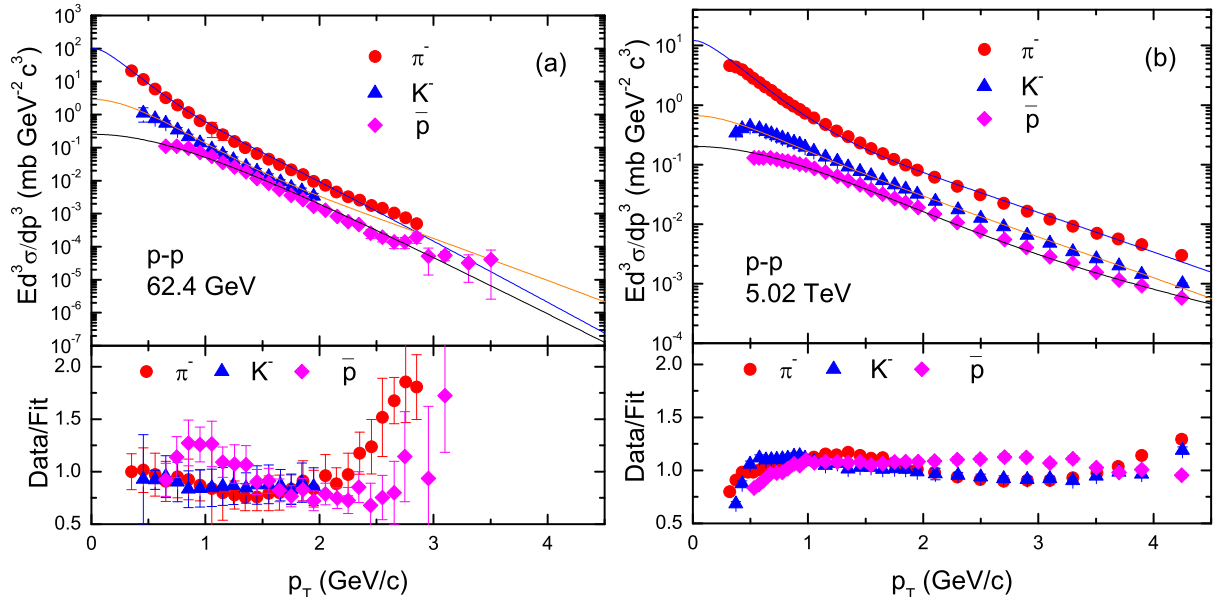


Fig. 3. Transverse momentum spectra of π^- , K^- and \bar{p} produced in pp collisions at (a) $\sqrt{s} = 62.4$ GeV and (b) $\sqrt{s} = 5.02$ TeV. The symbols represent the experimental data measured in the mid-pseudorapidity range $|\eta| < 0.35$ by the PHENIX Collaboration [33] and in the mid-rapidity range $|y| < 0.5$ by the ALICE Collaborations [32]. The curves are our results fitted by Eq. (4) with $l = 2$. Following each panel, the results of Data/Fit are presented.

particles. This leads to a volume differential freeze-out scenario and indicates different freeze-out surfaces for different particles, depending on their masses that show the early freeze-out of heavier particles as compared to the lighter particles [8, 9].

Figure 6 shows the dependences of effective temperature T on kinetic freeze-out volume V for productions of negative charged particles in (a) central and peripheral Au-Au collisions as well as in pp collisions at 62.4 GeV, and in (b) central and peripheral Pb-Pb collisions as well as in pp collisions at 5.02 TeV. The filled, empty and half filled symbols represent central and peripheral AA and pp collisions respectively. One can see that the effective temperature decreases with the increase of the kinetic freeze-out volume in central and peripheral AA and pp collisions. This result is natural due to the fact that a large kinetic freeze-out volume corresponds to a long kinetic freeze-out time and then a cool system and a low effective temperature.

From Figs. 4–6 one can also see that the effective temperature T and kinetic freeze-out volume V obtained from collisions at the LHC are larger than those obtained from collisions at the RHIC. These results are natural due to more violent collisions happening at higher energy. However, from the RHIC to the LHC, the increase of collision energy is obviously large,

and the increases of T and V are relatively small. This reflects the penetrability of projectile in the transparent target.

To study further the dependences of effective temperature T and kinetic freeze-out volume V on centrality and collisions energy, Table 2 contains the values of average T ($\langle T \rangle$) and average V ($\langle V \rangle$) for different types of collisions at the RHIC and LHC. These averages are obtained by different particle weights due to different contribution fractions of π^- , K^- and \bar{p} . One can see clearly that $\langle T \rangle$ and $\langle V \rangle$ at the LHC are larger than those at the RHIC. Generally, the effective temperature T happens between the chemical freeze-out temperature T_{ch} and kinetic freeze-out temperature T_{kin} . In particular, T_{ch} in central AA collisions is about 160 MeV, and T_{kin} in central AA collisions is less than 130 MeV [23, 24, 36, 37]. However, the values of $\langle T \rangle$ in Table 2 are larger because of Eq. (4) being used. In fact, Eq. (4) can be regarded as a different thermometer from literature [23, 24, 36, 37], which results in different effective temperature which is beyond the range of $[T_{ch}, T_{kin}]$.

Although the absolute values of effective temperature obtained in the present work are possibly inconsistent with T_{ch} and T_{kin} , the relative values of effective temperature are clearly worth considering. The present work shows that the effective temperature T and the ki-

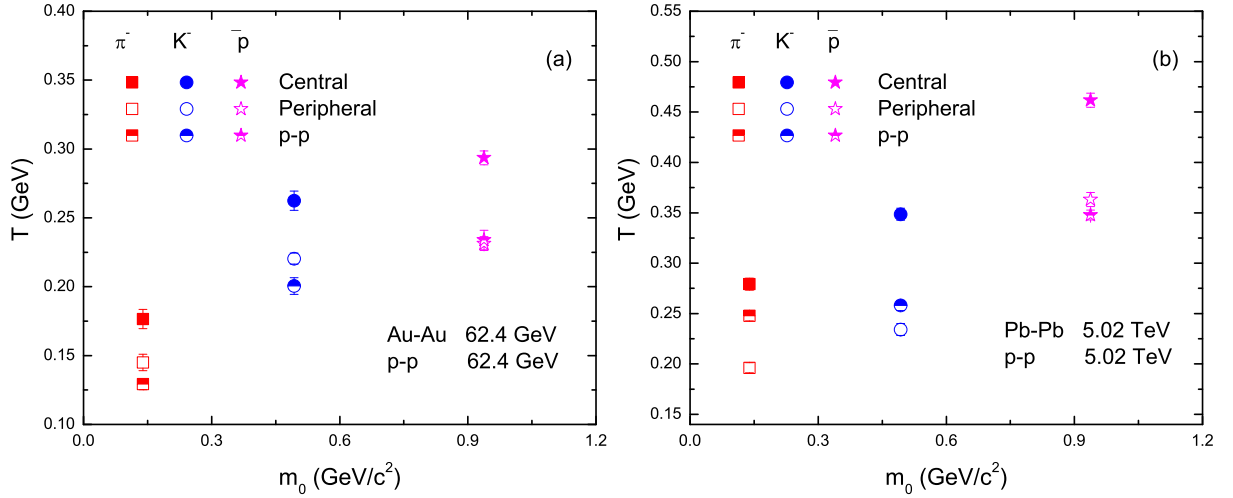


Fig. 4. Dependences of T on m_0 for negative charged particles produced in (a) central and peripheral Au-Au collisions as well as pp collisions at 62.4 GeV, and in (b) central and peripheral Pb-Pb collisions as well as pp collisions at 5.02 TeV. The filled, empty and half filled symbols represent central and peripheral AA and pp collisions respectively.

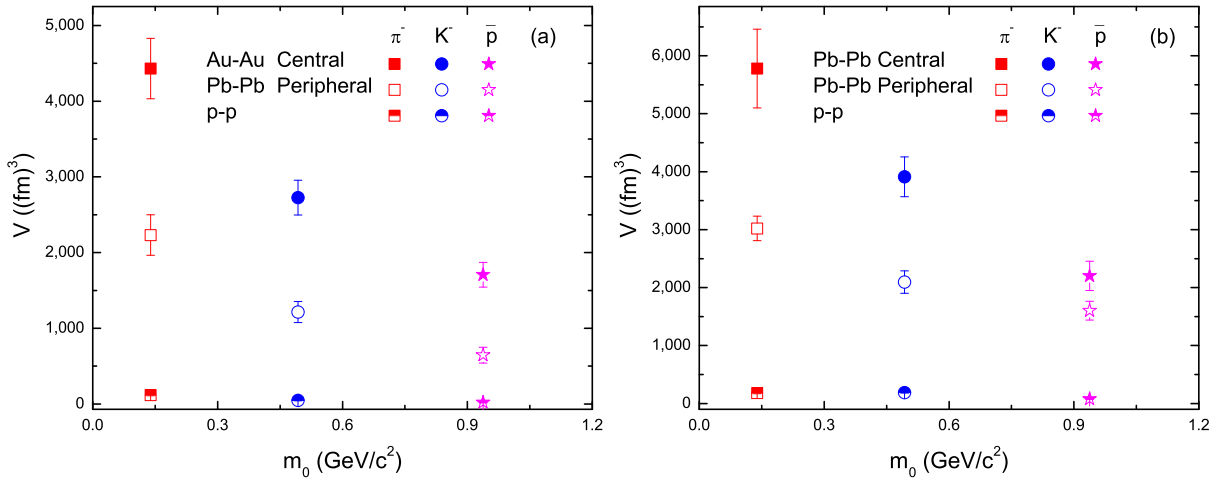


Fig. 5. Same as Fig. 4, but showing the dependences of V on m_0 .

netic freeze-out volume V in central and peripheral Pb-Pb and pp collisions at 5.02 TeV are larger than those in central and peripheral Au-Au and pp collisions at 62.4 GeV. This shows their strong dependence on collision energy. Furthermore, both T and V in central and peripheral Pb-Pb collisions are larger than those in central and peripheral Au-Au collisions that also shows somehow their dependence on size of the system, though this dependence can be neglected due to small difference in their size. The dependences of collision energy and system size are not discussed here in detail because of the unavailability of wide range of data but it can be focused in the future work.

Before summary and conclusions, we would like to point out that the method that the source volume can be extracted from the transverse momentum spectra of identified particles is approximately effective in high energy collisions. At high energy (dozens of GeV and above), the particle dependent chemical potentials are less than several MeV which affects less the source volume. Eqs. (1)–(4) can be used approximately. This renders that our result for pp collisions is larger than that ($\sim 34 \text{ fm}^3$) by the femtoscopy method with two-pion Bose-Einstein correlations [38]. At intermediate and low energies, the method used here is possibly unsuitable due to the fact that the particle dependent

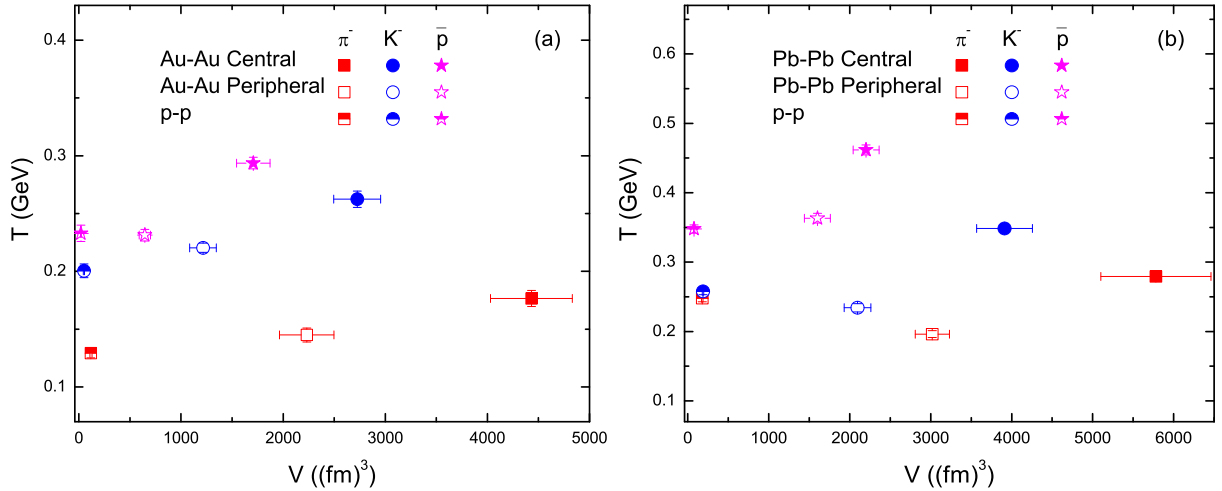


Fig. 6. Same as Fig. 4, but showing the dependences of T on V .

Table 2. Values of $\langle T \rangle$ and $\langle V \rangle$ in different types of collisions at the RHIC and LHC. The average values are obtained by different weights due to different contribution fractions of π^- , K^- and \bar{p} .

| Collisions | $\sqrt{s_{NN}}$ (\sqrt{s}) | $\langle T \rangle$ (GeV) | $\langle V \rangle$ (fm^3) |
|------------------|--------------------------------|---------------------------|---------------------------------------|
| Central Au-Au | 62.4 GeV | 0.213 ± 0.005 | 3644 ± 155 |
| Peripheral Au-Au | 62.4 GeV | 0.164 ± 0.004 | 1967 ± 61 |
| pp | 62.4 GeV | 0.146 ± 0.004 | 102 ± 4 |
| Central Pb-Pb | 5.02 TeV | 0.311 ± 0.006 | 5033 ± 213 |
| Peripheral Pb-Pb | 5.02 TeV | 0.216 ± 0.005 | 2739 ± 98 |
| pp | 5.02 TeV | 0.260 ± 0.005 | 170 ± 7 |

chemical potentials at the kinetic freeze-out are large and unavailable. In general, the particles of different species develop different chemical potentials from chemical freeze-out to kinetic freeze-out. In addition, different particles correspond to different source temperatures which result in mass or particle dependent differential kinetic freeze-out scenario [2, 3, 18, 34, 35].

4 Summary and conclusions

We summarize here our main observations and conclusions

(a) The extracted parameters from the transverse momentum spectra of identified particles produced in central and peripheral Au-Au collisions at 62.4 GeV and Pb-Pb collisions at 5.02 TeV are studied. Furthermore, the same analysis is done for pp collisions at both RHIC and LHC energies. The two-component standard distribution is used, which includes both the very soft and soft excitation processes. The effective temperature and kinetic freeze-out volume are larger in central collisions

as compared to peripheral collisions which show large number of participant nucleons in central collisions and it undergoes a quick equilibrium state.

(b) The effective temperatures in the central and peripheral Au-Au (Pb-Pb) collisions at the RHIC (LHC) is observed to increase with increasing the mass of the particles, which shows a mass differential kinetic freeze-out scenario at RHIC and LHC energies. The kinetic freeze-out volume decrease with the increase of mass that shows different kinetic freeze-out volumes for different particles and it indicates the volume dependent differential kinetic freeze-out scenario.

(c) The effective temperatures in peripheral Au-Au and pp collisions at 62.4 GeV as well as in peripheral Pb-Pb and pp collisions at 5.02 TeV are respectively equivalent and have the same trend, which show the same thermodynamic nature of the parameters in peripheral AA and pp collisions at the same center-of-mass energy (per nucleon pair). The effective temperatures in both central and peripheral AA and pp collisions decrease with the increase of the kinetic freeze-out volume

in the considered energy range.

(d) Both the effective temperature and kinetic freeze-out volume in central and peripheral AA and pp collisions at the LHC are larger than those at the RHIC, which shows their dependence on collision energy. Also, central (peripheral) Pb-Pb collisions give larger effective temperature and kinetic freeze-out volume than central (peripheral) Au-Au collisions which show somehow their dependence on the size of the system, which can be neglected due to small difference in their sizes.

Data Availability

The data used to support the findings of this study are included within the article and are cited at relevant places within the text as references.

Ethical Approval

The authors declare that they are in compliance with ethical standards regarding the content of this paper.

Disclosure

The funding agencies have no role in the design of the study; in the collection, analysis, or interpretation of the data; in the writing of the manuscript; or in the decision to publish the results.

Conflicts of Interest

The authors declare that there are no conflicts of interest regarding the publication of this paper.

Acknowledgments

This work was supported by the National Natural Science Foundation of China under Grant No. 11575103, the Chinese Government Scholarship (China Scholarship Council), the Scientific and Technological Innovation Programs of Higher Education Institutions in Shanxi (STIP) under Grant No. 201802017, the Shanxi Provincial Natural Science Foundation under Grant No. 201701D121005, and the Fund for Shanxi “1331 Project” Key Subjects Construction.

References

- [1] N. Xu for the STAR Collaboration, *Nucl. Phys. A* **931**, 1 (2014).
- [2] S. Chatterjee, S. Das, L. Kumar, D. Mishra, B. Mohanty, R. Sahoo, N. Sharma, *Adv. High Energy Phys.* **2015**, 349013 (2015).
- [3] S. Chatterjee, B. Mohanty, R. Singh, *Phys. Rev. C* **92**, 024917 (2015).
- [4] S. Chatterjee, B. Mohanty, *Phys. Rev. C* **90**, 034908 (2014).
- [5] S.S. Räsänen for the ALICE Collaboration, *EPJ Web Conf.* **126**, 02026 (2016).
- [6] G. Bertsch, P.J. Siemens, *Phys. Lett. B* **126**, 9 (1983).
- [7] L.G. Moretto, G.J. Wozniak, *Ann. Rev. Nucl. Part. Sci.* **43**, 379 (1993).
- [8] D. Thakur, S. Tripathy, P. Garg, R. Sahoo, J. Cleymans, *Acta Phys. Polon. Supp.* **9**, 329 (2016).
- [9] D. Thakur, S. Tripathy, P. Garg, R. Sahoo, J. Cleymans, *Adv. High Energy Phys.* **2016**, 4149352 (2016).
- [10] D.H.E. Gross, *Phys. Rept.* **279**, 119 (1997).
- [11] Borderie, *J. Phys. G* **28** R217 (2002).
- [12] M. D’Agostino, F. Gulminelli, Ph. Chomaz, M. Bruno, F. Cannata, R. Bougault, F. Gramegna, I. Iori, N. Le Neindre, G.V. Margagliotti, A. Moroni, G. Vannini, *Phys. Lett. B* **473**, 219 (2000).
- [13] M. D’Agostino, R. Bougault, F. Gulminelli, M. Bruno, F. Cannata, Ph. Chomaz, F. Gramegna, I. Iori, N. Le Neindre, G.V. Margagliotti, A. Moroni, G. Vannini, *Nucl. Phys. A* **699**, 795 (2002).
- [14] P. Chomaz, V. Duflot, F. Gulminelli, *Phys. Rev. Lett.* **85**, 3587 (2000).
- [15] R. Hagedorn, *Riv. Nuovo Cimento* **6**(10), 1 (1983).
- [16] J. Cleymans, D. Worku, *Eur. Phys. J. A* **48**, 160 (2012).
- [17] H. Zheng, L.L. Zhu, *Adv. High Energy Phys.* **2016**, 9632126 (2016).
- [18] Z.B. Tang, Y.C. Xu, L.J. Ruan, G. van Buren, F.Q. Wang, Z.B. Xu, *Phys. Rev. C* **79**, 051901(R) (2009).
- [19] E. Schnedermann, J. Sollfrank, U. W. Heinz, *Phys. Rev. C* **48**, 2462 (1993).
- [20] H.-L. Lao, F.-H. Liu, B.-C. Li, M.-Y. Duan, *Nucl. Sci. Tech.* **29**, 82 (2018).
- [21] B.I. Abelev *et al.* [STAR Collaboration], *Phys. Rev. C* **79**, 034909 (2009).
- [22] B.I. Abelev *et al.* [STAR Collaboration], *Phys. Rev. C* **81**, 024911 (2010).
- [23] J. Cleymans, H. Oeschler, K. Redlich, S. Wheaton, *Phys. Rev. C* **73**, 034905 (2006).
- [24] A. Andronic, P. Braun-Munzinger, J. Stachel, *Nucl. Phys. A* **772**, 167 (2006).
- [25] S. Uddin, J.S. Ahmad, W. Bashir, R.A. Bhat, *J. Phys. G* **39**, 015012 (2012).
- [26] R.P. Adak, S. Das, S.K. Ghosh, R. Ray, S. Samanta, *Phys. Rev. C* **96**, 014902 (2017).
- [27] R. Odorico, *Phys. Lett. B* **118**, 151 (1982).

- [28] K. Aamodt *et al.* [ALICE Collaboration], *Phys. Lett. B* **693**, 53 (2010).
- [29] M. Biyajima, T. Mizoguchi, N. Suzuki, *Int. J. Mod. Phys. A* **32**, 1750057 (2017).
- [30] H.-L. Lao, Y.-Q. Gao, F.-H. Liu, *Adv. High Energy Phys.* **2020**, 5064737 (2020).
- [31] M. Shao for the STAR Collaboration, *J. Phys. G* **31**, S85 (2005).
- [32] Y.C. Morales, N. Hussain, N. Jacazio, A. Ortiz I. Ravasenga, O. Vázquez, G. Volpe, CERN Preprint ALICE-ANA-2016-xxx (July 12, 2017).
- [33] A. Adare *et al.* [PHENIX Collaboration], *Phys. Rev. C* **83**, 064903 (2011).
- [34] M. Waqas, F.-H. Liu, S. Fakhraddin, M.A. Rahim, *Indian J. Phys.* **93**, 1329 (2019).
- [35] M. Waqas, F.-H. Liu, arXiv:1806.05863 [hep-ph] (2018).
- [36] A. Andronic, P. Braun-Munzinger, J. Stachel, *Acta Phys. Pol. B* **40**, 1005 (2009).
- [37] A. Andronic, P. Braun-Munzinger, J. Stachel, *Nucl. Phys. A* **834**, 237c (2010).
- [38] K. Aamodt *et al.* [ALICE Collaboration], *Phys. Rev. D* **84**, 112004 (2011).